nature geoscience
SUPPLEMENTARY INFORMATION
DOI: 10.1038/NGEO901

S.1 Ocean Model Experiments

S.1a: The HYbrid Coordinate Ocean Model (HYCOM)

The HYCOM is a primitive equation OGCM with a hybrid vertical coordinate that is isopycnal in the open, stratified ocean, terrain-following coordinates in shallow coastal regions, and z-coordinates in the mixed layer and unstratified seas[1]. It has been applied to IO[2-5], Indo-Pacific basin with half a degree resolution[6] and tropical Atlantic Ocean studies[7]. Here, HYCOM is configured to the Indo-Pacific basin (30 ^{o}E - 290 ^{o}E, 55 ^{o}S - 55 ^{o}N) with 0.33°x0.33° horizontal resolution and 20 vertical layers. Bottom topography is from ETOPO5 with 2° x 2° smoothing. The southern and northern ocean boundaries are closed and sponge layers of 5° are applied that relax model temperature and salinity fields to Levitus climatology. The K-Profile Parameterization (KPP) is used for boundary layer mixing[8-9] and no slip conditions are applied along continental boundaries.

The HYCOM was spun–up from a state of rest for 30 years using COADS (Comprehensive Ocean-Atmosphere Dataset) monthly climatology fields, and then integrated forward in time using 3-day-mean ERA40 (European Center for Medium-Range Weather Forecasts 40-year Reanalysis)[10] forcing fields for the period of 1958-2001 when ERA40 fields are available. Restarting from January 1st 2000, the experiment was extended from 2000 to 2008 using 3-day-mean winds from QuikSCAT satellite data[11], net long and shortwave radiative fluxes from the International Satellite Cloud Climatology Project flux data (ISCCP-FD)[12], National Center for Environmental Prediction (NCEP; hereafter referred to as NCEP1)[13] air temperature and specific humidity, and Climate Prediction

DOI: 10.1038/NGEO901

Center (CPC) Merged Analysis of Precipitation (CMAP) pentad precipitation[14]. Wind speed, air temperature, specific humidity and model SST are used to calculate surface turbulent heat fluxes. The sea level anomaly (SLA) from the extended solution for 2002-2008, together with the solution for 1961-2001 forced by ERA40 fields, is shown in Figs 1 and 2. Note that even though the model SLA agrees well with the observations, transient response can be excited due to switching of forcing fields. To reduce this effect, we use the extended solution starting in 2002. In addition, differences between ERA40 and QuikSCAT winds can also affect the trend analysis of winds. Consequently, the paper focuses on analyzing the results of 1961-2001 periods.

The SLA from HYCOM includes dynamical effects (mainly wind-driven mass redistribution), thermal expansion and salinity effects. The effect of continental ice retreat is not included in HYCOM and any other models used in this paper.

S.1b The Parallel Ocean Program (POP)

The POP used here is the ocean component of the National Center for Atmospheric Research (NCAR) Community Climate System Model version 4 (CCSM4). It is a z-coordinate, primitive equation global ocean model based on the POP developed at the Los Alamos National Laboratory[15]. The curvilinear horizontal mesh has 320 zonal and 384 meridional grid points with its northern grid pole displaced into Greenland. The vertical grid resolution is 60 levels[16]. Here POP is forced by the interannually varying forcing dataset (CORE.2-IAF) [17], spanning 1948–2006. Surface fluxes are computed from bulk formulae using the prognostic ocean model SST and an observed atmospheric state.

The prescribed atmosphere is a combination of 6-hourly atmospheric state data from NCEP1 reanalysis, daily radiation from the ISCCP-FD[12], monthly merged precipitation from CMAP precipitation and the Global Precipitation Climatology Project (GPCP)[18], and climatological continental river runoff. The raw forcing data have been adjusted to ameliorate known systematic biases. The initial condition for the experiment is a state of rest, with temperature and salinity prescribed from the global climatological distribution of the 1998 World Ocean Atlas[19], and run for 3 cycles using 1948-2004 forcing fields. The last cycle data are analyzed and shown in Figs S2 and S3. Its sea level change is dynamical and results mainly from wind-driven mass redistribution. Effects of thermal expansion and salinity effects should be calculated offline.

S.1c Linear Model (LM)

The linear continuously stratified ocean model is described in detail previously[20], and it has been applied to several Indian and Atlantic Ocean studies[2,3,7]. In this paper, it is set up for the Indo-Pacific basin (30 ^{o}E - 290 ^{o}E, 45^{o}S-45^{o}N) with 0.33^{o} x 0.33 ^{o} horizontal resolution as that of HYCOM. The equations of motion are linearized about a state of rest with a realistic background stratification calculated from the Levitus temperature and salinity averaged over 20^{o}S-20^{o}N of the Indo-Pacific basin[19]. The ocean bottom is assumed to be flat. With these restrictions, solutions can be represented as expansions in vertical normal modes of the system, with the total solution being the sum of all modes. In this paper, the first 15 baroclinic modes are used with sea level changes dominated by the first two. Closed boundaries are applied at the northern and southern ocean boundaries and a damper on zonal currents is applied within 5^{o} of the boundaries to damp

DOI: 10.1038/NGEO901

the currents toward zero, in order to reduce the spurious coastal Kelvin waves caused by the artificial boundaries. This is basically consistent with the sponge layer of HYCOM for the corresponding regions.

As with HYCOM, the LM was first spun up for 30 years using the monthly climatology of COADS wind stress forcing. Restarting from year 30, the model was integrated forward with 3-day mean ERA40 wind stress forcing for the period of 1958-2001. This solution is referred to as LM MR (main run). A parallel experiment – LM EXP run – is performed, in which the Pacific wind stress is fixed to the 1958-2001 mean. Sea level change in this solution, therefore, results mainly from the IO wind forcing. Their sea level trends are shown in Fig. S3.

S.2 AGCM Experiments and Climate Model Solutions

AGCMs and Experiments: Two AGCMs are used to perform idealized experiments. One is the Geophysical Fluid Dynamics Laboratory (GFDL) global atmosphere model AM2.1[21], with spatial resolution of 2.5^{o} in longitude, ~2^{o} in latitude and 24 vertical levels. The other is the Global Forecast System (GFS) model, which is the atmospheric component of the NCEP Climate Forecast System (CFS) [22]. The GFS model was run with spatial resolution of T62 (~1.9^{o} x 1.9^{o}) and 64 vertical levels.

For each model, one control run (CR) and two idealized experiment runs (EXP1 and EXP2) were performed. The CR was forced by the global monthly climatology of HadISST, and the last 50-year mean was taken as the CR solution. EXP1 initialized from

October 1st of a random year from the 50-year CR solution, and integrated forward for 15 years and 3 months using idealized SST forcing - the linear trend of SST for the period of 1977-2006 in the warm pool region (Fig. S6A) superimposed onto the global monthly SST climatology (global SST climatology + 30yr x trend in the warm pool). EXP2 is similar to EXP1 but initialized from October 1st of a different year. The 30-year mean from EXP1 and EXP2 was then used as the EXP solution for each model. The difference between EXP and CR solutions isolates the effects of SST trend forcing. The AGCM winds shown in Figs 3 and S4 are the 60-member ensemble from the two models forced by the warm pool (40°E-180°E, 25°S-25°N) SST trend.

We also forced the two AGCMs by global SST trend and tropical-subtropical (0-360°E, 25°S-25°N) SST trend. The trends of surface wind stress, Ekman pumping velocity, Hadley and Walker circulations over the IO region from these experiments are similar to those of shown in Figs 3 and S4, except for somewhat weaker amplitudes. This further suggests that the circulation changes discussed above result mainly from warming in the Indo-Pacific warm pool region in the past few decades.

Climate model solutions: Surface wind and sea level from CCSM3 and PCM are also analyzed. Two of the 9 ensemble members actually produce sea level patterns similar to those observed over the IO region, although the 9-member ensemble mean does not (not shown). This is promising, given that the IO circulation is such a regional feature, and it is even challenging for global climate models to simulate the mean seasonal cycle of monsoon circulation (Kevin Trenberth, 2009, Pers. Commu.). Even though climate models

DOI: 10.1038/NGEO901

are able to produce the anthropogenic warming in the Indo-Pacific warm pool region (Fig. 3D), they may not be able to reproduce the observed atmospheric circulation changes. These results, although may partly reflect the effects of natural variability, point to our need for further developing and improving realistic representation of the complex processes in the climate system - such as improving atmospheric convection schemes - in order to warrant a reliable regional prediction of future climate. Since climate models already do well at simulating global scale aspects of sea level rise due to thermal expansion (*1 of main text reference*), as well as the regional response of tropical-subtropical SSTs to anthropogenic forcing (Fig. 3D), it is very possible that the models could be used to predict time-evolving regional changes in sea level in the near future. This possibility should be explored after reliable ice sheet models are developed and included[23].

S.3 Tide Gauge data, Melting Land Ice, and Reconstructed Sea Level

Tide Gauge Data: The Global Positioning System (GPS) land movement data within 40km of the tide gauge stations[24] are available only at station Fremantle since 1994. For the sake of consistency, only GIA model data are used for land movement correction. Vertical land movement, unfortunately, can be a major cause for model/data differences. For example, at station Diamond Harbor in the northern Bay of Bengal, tide gauge observed sea level trend is more than 4 times larger than that of HYCOM solution, and it is also substantially larger than those of adjacent stations. This large rate of sea level rise may result from the large tectonic subsidence rate of ~ 4mm/yr in River Ganga Delta[25] where the tide gauge is located. This station was excluded in an estimate of mean sea level rise (*3 of main text reference*), based on a consistency check along the North IO coasts according

to large-scale ocean dynamics[26]. For the same reason, we also excluded this station in our analysis.

Melting continental ice: As discussed in the main text, melting of continental glaciers, ice caps, Greenland and Antarctic ice sheets will increase the mass of freshwater in the ocean and thus increase global sea level. If we uniformly add the observed estimate of 6.9±7.1 cm/century sea level rise for the 1961-2003 period (glaciers and ice caps 0.50±0.18, Greenland ice sheet 0.05±0.12, and Antarctic ice sheet 0.14±0.41) from IPCC AR4 to HYCOM solution over the Indian Ocean (*Fig. 1 of main text*), the model/data agreements will improve in some stations of the north IO (such as Ko Taphao Noi and Vishakhapatnam), but HYCOM sea level will be much higher than that of tide gauge data in the south Indian Ocean. It remains unclear how to reconcile this discrepancy. This may, however, indicate the possible "non-uniform" influence of melting land ice on regional sea level (*2 of main text reference*), in addition to the land movement effect on tide gauge data and uncertainties in the models and their forcing fields. It is not known how the combined melting of Antarctic and Greenland ice sheets, continental glaciers and icecaps in the real world will affect the spatial variations of IO sea level change.

Reconstruction: Reconstructed sea level data by Church et al. (*8 of main text reference*) are also analyzed, and the 1961-2001 trend is similar to Fig. 15 of Church et al. Relative lows of sea level rise are shown in the sea level fall region, although the reconstructed sea level trends do not show negative values, likely because the tide gauge records used to reconstruct temporal variations of sea level are available only after 1990 in the region.

DOI: 10.1038/NGEO901

S.4 References

1. Bleck, R. An oceanic general circulation model framed in hybrid isopycnic-Cartesian coordinates. Ocean Modeling. *Ocean Modeling* **4**, 55-88 (2002).

2. Han, W. *et al*. Impact of atmospheric intraseasonal variability in the Indian Ocean: low-frequency rectification in equatorial surface current and transport. *J. Phys. Oceanogr.* **34**, 1350-1372 (2004).

3. Han, W. Origins and dynamics of the 90-day and 30-60 day variations in the equatorial Indian Ocean. *J. Phys. Oceanogr.* **35**, 708-728 (2005).

4. Han, W. *et al*. Impact of atmospheric intraseasonal oscillations on the Indian Ocean dipole during the 1990s. *J. Phys. Oceanogr.* **36**, 670-690 (2006).

5. Han, W. *et al.* Intraseasonal variability of Indian Ocean sea surface temperature during boreal winter: Madden-Julian Oscillation versus submonthly forcing and processes. *J. Geophys. Res*., **112**, C04001 (2007).

6. Trenary, L.L. & Han, W. Causes of decadal subsurface cooling in the tropical Indian Ocean during 1961-2000. *Geophys. Res. Lett*. **35**, L17602 (2008).

7. Han, W. *et al.* Dynamics of intraseasonal sea level and thermocline variability in the equatorial Atlantic during 2002-2003. *J. Phys. Oceanogr.* **38**, 945-967 (2008).

8. Large, W.G. *et al*. Oceanic vertical mixing: A review and a model with a nonlocal boundary layer parameterization. *Rev. Geophys.* **32**, 363-403 (1994).

9. Large, W.G. *et al*. Sensitivity to surface forcing and boundary layer mixing in a global ocean model: Annual-mean climatology. *J. Phys. Oceanogr*. **27**, 2418-2447 (1997).

10. Uppala, S.M. *et al*. The ERA-40 reanalysis. *Quart. J. Roy. Meteor. Soc.*, **131**, 2961-3012 (2005).

11. Tang, W. & Liu, W.T. Objective interpolation of scatterometer winds. *JPL publication 96-19, Jet Propulsion Laboratory, Pasadena, CA*, 16pp (1996)

12. Zhang, Y. *et al*. Calculation of radiative fluxes from the surface to top of atmosphere based on ISCCP and other global data sets: Refinements of the radiative transfer model and the input data. *J. Geophys. Res.* **109**, D19105 (2004).

13. Kalnay, E. *et al*. The NCEP/NCAR 40-year reanalysis project. *Bull. Amer. Meteor. Soc.*, **77**, 437-471 (1996).

14. Xie, P. & Arkin, P.A. Analyses of global monthly precipitation using gauge observations, satellite estimates, and numerical model predictions. *J. Clim.,* **9**, 840-858 (1996).

15. Smith, R.D. *et al.,* Parallel ocean general circulation modeling. *Physica* **D 60**, 38-61 (1992).

16. Yeager, S.G. & Jochum, M. The connection between Labrador Sea buoyancy loss, deep western boundary current strength, and Gulf Stream path in an ocean circulation model. *Ocean Modelling*, **30**, 207-224 (2009).

17. Large, W.G. & Yeager, S.G. The global climatology of an interannually varying air-sea flux data set. *Clim. Dyn*., **33**, 341-364 (2009).

18. Huffman, G. *et al.* The global precipitation climatology project (GPCP) combined precipitation dataset. *Bull. Am. Meteor*. Soc. **78**, 5-20 (1997).

DOI: 10.1038/NGEO901

19. Levitus, S. *et al*. Yearly and year-season upper ocean temperature anomaly fields, 1948-1998. *NOAA Atlas NESDIS* **18**, pp. 346 (1998).

20. McCreary, J.P. A linear, stratified ocean model of the equatorial undercurrent. *Philos. Trans. R. Soc. London Ser. A*. **298**, 603-635 (1981).

21. The GFDL Global Atmospheric Model Development Team. The new GFDL global atmosphere and land model AM2-LM2: evaluation with prescribed SST simulations. *J. Clim.*, **17**, 4641-4673 (2004).

22. Saha, S. *et al*., The NCEP climate forecast system. *J. Clim*., **24**, 3483-3517 (2006).

23. Rahmstorf, S. *et al.* Recent climate observations compared to projections. *Science*, **316**, 709 (2007).

24. Mazzotti, S. *et al*. Relative and absolute sea level rise in western Canada and northwestern United States from a combined tide gauge-GPS analysis. *J. Geophys. Res.,* **113***,* C11019 (2008).

25. Goodbred, S.L. & Kuel, S.A., The significance of large sediment supply, active tectonism, and eustasy on margin sequence development: late quarternary stratigraphy and evolution of the Ganges-Brahmaputra delta. *Sediment. Geol*., **133**, 227-248 (2000).

26. Clarke, A.J. & Liu, X. Interannual sea level in the northern and eastern Indian Ocean. *J. Geophys. Res*., **99**, 1224-1235 (1994).

27. Bosilovich, M. NASA's model Era retrospective-analysis for research and applications: integrating Earth observations. *Earthzine* (2008).

28. Bosilovich, M. *et al*. Evaluation of global precipitation in reanalyses. *Journal of Applied Meteorology and Climatology* **47**, 2279-2299 (2008).

29. Onogi, K. *et al.* The JRA-25 reanalysis. *J. Meteor. Soc. Japan*, **85**, 369-432 (2007).

30. Kanamitsu, M. *et al*. NCEP-DOE AMIP-II reanalysis (R-2). *Bull. Amer. Meteor. Soc.*, **83**, 1631-1643 (2002).

S.5 Figures

Fig. S1. A) December, January, February (DJF) mean ERA40 surface wind stress (arrow) and Ekman pumping velocity (10^{-4}cms^{-1}; color contour) averaged for 1961-2001 period; B) same as A) except for June, July, August (JJA) mean; C) Kendall Theil trends of DJF wind stress and Ekman pumping velocity (10^{-4}cms^{-1}century^{-1}) for 1961-2001; D) same as C) except for JJA; E) and F) are the same as C) and D) except for NCEP1 reanalysis winds. Black (red) arrows in C)-F) are above (below) 95% significance.

Fig. S2. A) DJF mean HYCOM SLA (with basin mean removed to emphasize the spatial pattern) averaged for 1961-2001; B) same as A) except for JJA; C) Kendall Theil trend of DJF HYCOM SLA for 1961-2001; D) same as C) except for JJA; E) and F) are the same as C) and D) except for SODA dynamical SLA trends, which result mainly from wind-driven mass-redistribution; G) and H) are the same as C) and D) except for POP dynamical SLA trends. White contours show 95% significance level.

Fig. S3. Kendall Theil trend of SLA for 1961-2001 from A) HYCOM; B) SODA (dynamical SLA corrected by global thermal expansion and salinity effects); SODA used POP, which is volume conserved and its dynamical SLA (mainly wind driven) requires correction; C) POP dynamical; D) SODA dynamical; E) wind-driven LM main run (MR);

DOI: 10.1038/NGEO901

and F) LM experiment run (EXP) forced only by IO wind variations. Light blue/green regions are below and the rest above 95% significance.

Fig. S4. A) Kendall Theil trend of atmospheric meridional overturning cell (local Hadley cell) for 1961-2001 from ERA40 winds zonally averaged for 45°E-95°E of the IO; only arrows above 95% significance are shown; B) same as a) except for zonal overturning cell (local Walker cell) averaged for 5°S-5°N; C) and D) are the same as A) and B) except for NCEP1 winds; E) and F) are the local Hadley and Walker cells from 60 member ensemble of idealized experiments using two AGCMs, GFDL AM2.1 and GFS models (see S.2), forced by the warm pool SST trend (Fig. S6). Units for zonal and meridonal wind trends are $ms^{-1}century^{-1}$, and for vertical wind trends are $0.005 \times pascal\ s^{-1}century^{-1}$.

Fig. S5. Kendall Theil trends of surface wind stress for 1979-2001 period when all data are available from five reanalysis products A) MERRA – Modern Era Retrospective-analysis for Research and Applications[27,28]; B) JRA25 - the Japanese 25-yr reanalysis[29]; C) ERA40; D) NCEP1; E) NCEP - Department of Energy (DOE) Reanalysis II (hereafter referred to as NCEP2)[30], F) ICOADS data. Black arrows are above and blue arrows are below 95% significance.

Fig. S6. A) Linear trend of HadISST for the periods of 1977-2006 in the Indo-Pacific warm pool (40°E-180°E, 25°S-25°N). This trend was added to the SST monthly mean climatology and then used to force the ACGMs (see S.2); B) The SST trend for 1979-2001, the period of winds shown in Fig. S5; it is similar to the trend shown in A); C) The SST

trend for 1961-2001, our period of interest as shown in Figs 3 and S3, also has similar spatial pattern but with some differences in magnitudes comparing to A) and B).

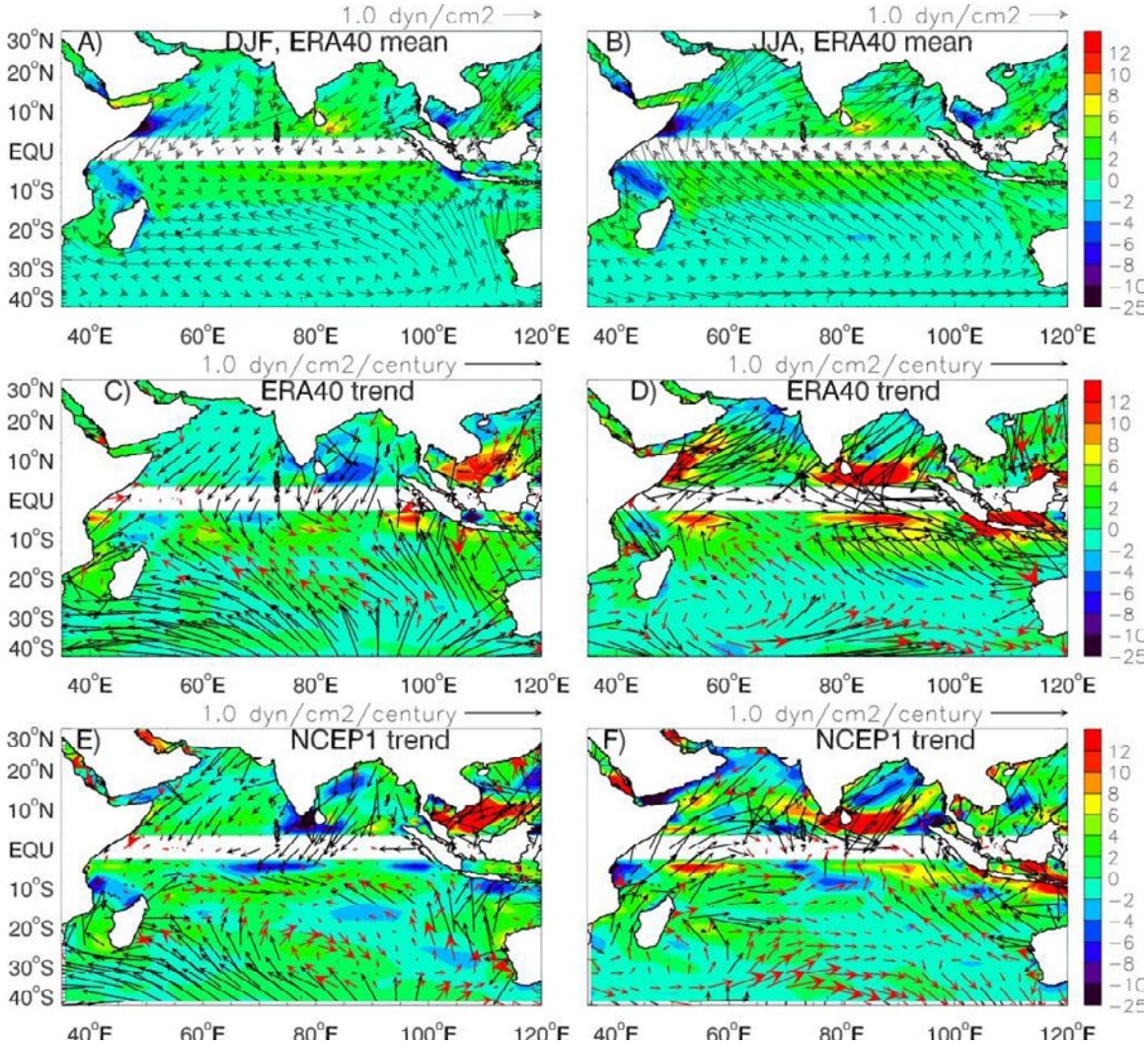

Fig. S1

DOI: 10.1038/NGEO901

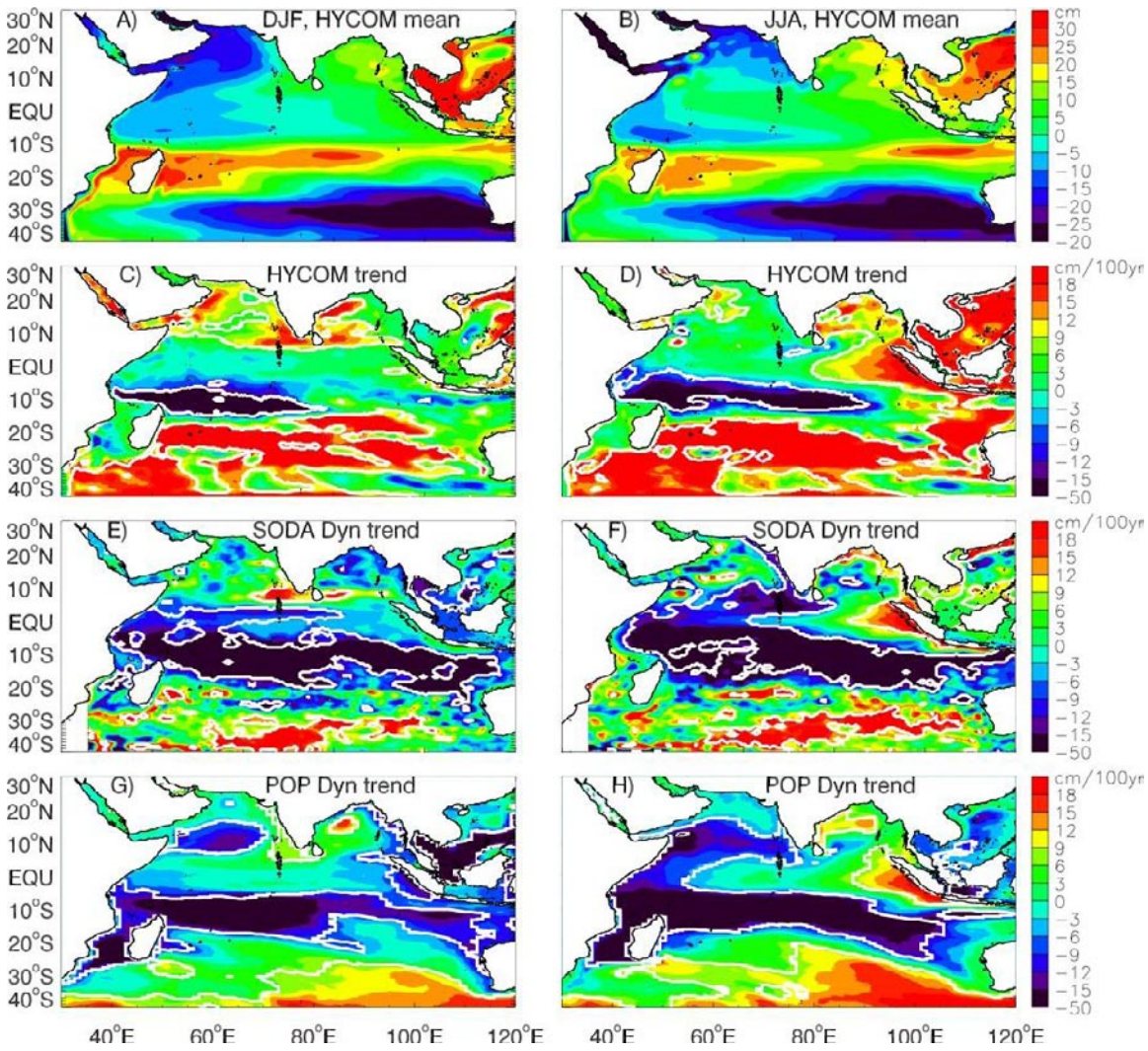

Fig. S2

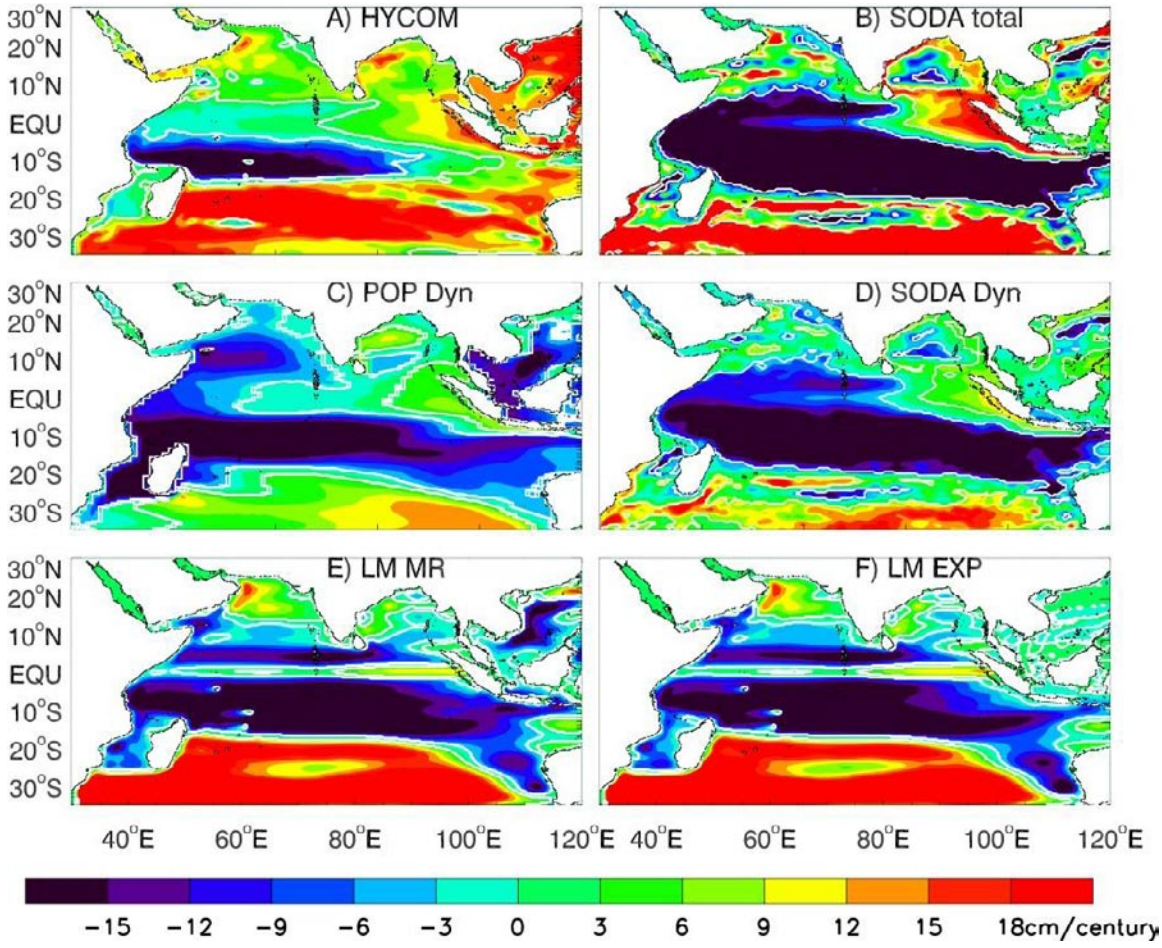
A) HYCOM
B) SODA total
C) POP Dyn
D) SODA Dyn
E) LM MR
F) LM EXP
30°N
20°N
10°N
EQU
10°S
20°S
30°S
40°E
60°E
80°E
100°E
120°E
−15 −12 −9 −6 −3 0 3 6 9 12 15 18cm/century

Fig. S3.

DOI: 10.1038/NGEO901

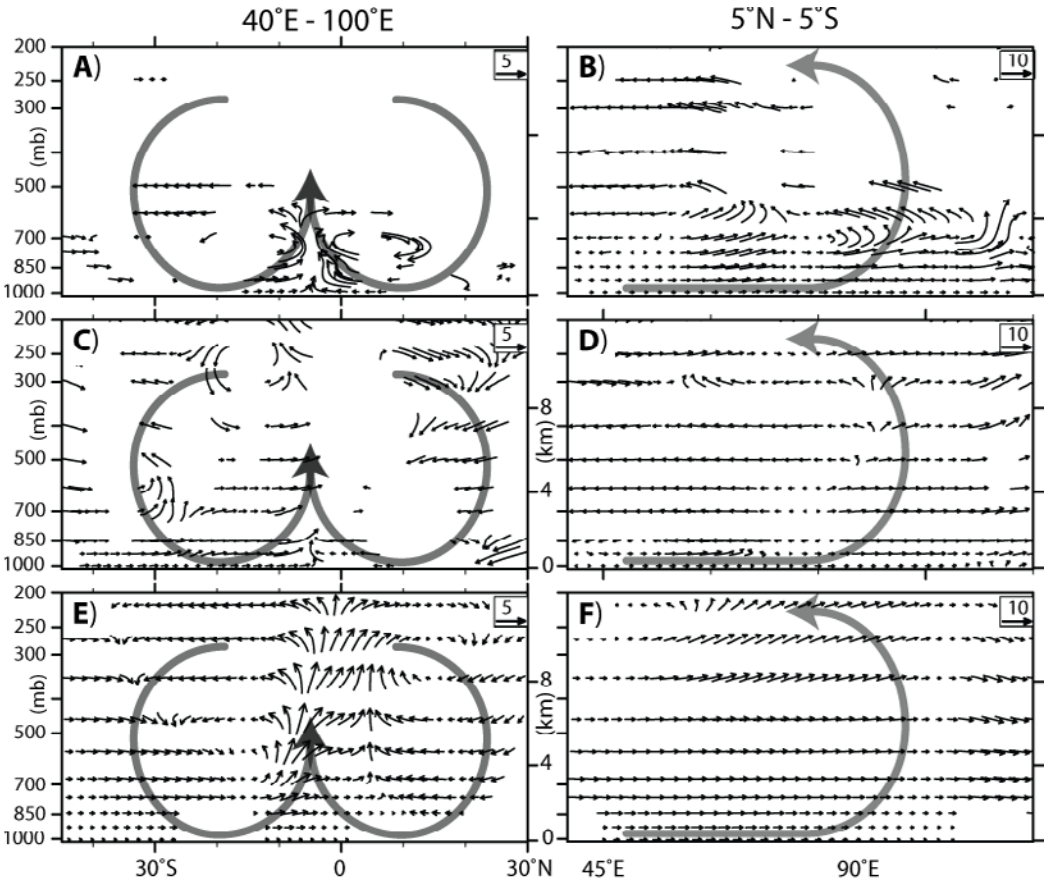

Fig. S4

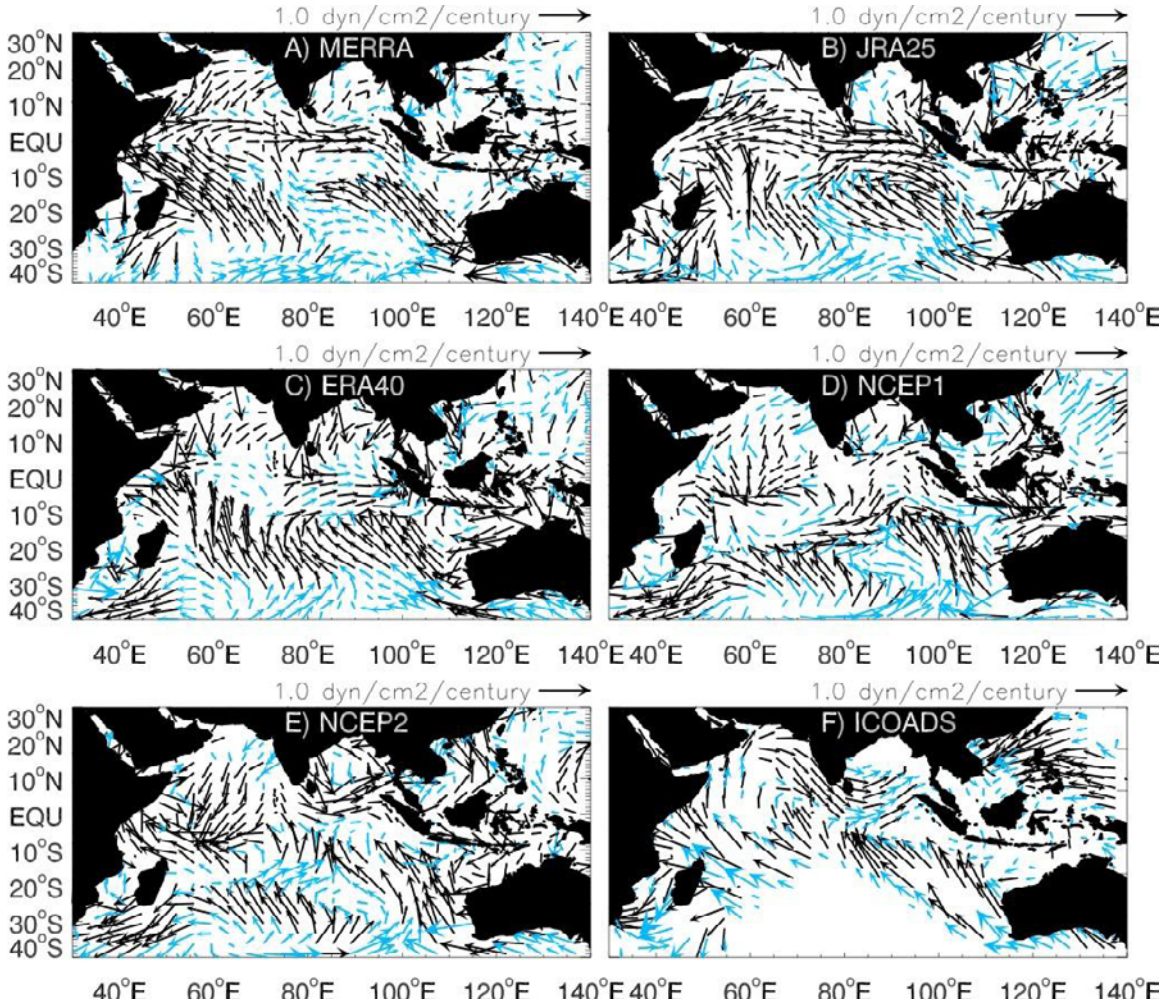
1.0 dyn/cm2/century
A) MERRA
B) JRA25
C) ERA40
D) NCEP1
E) NCEP2
F) ICOADS
30°N
20°N
10°N
EQU
10°S
20°S
30°S
40°S
40°E 60°E 80°E 100°E 120°E 140°E

Fig. S5

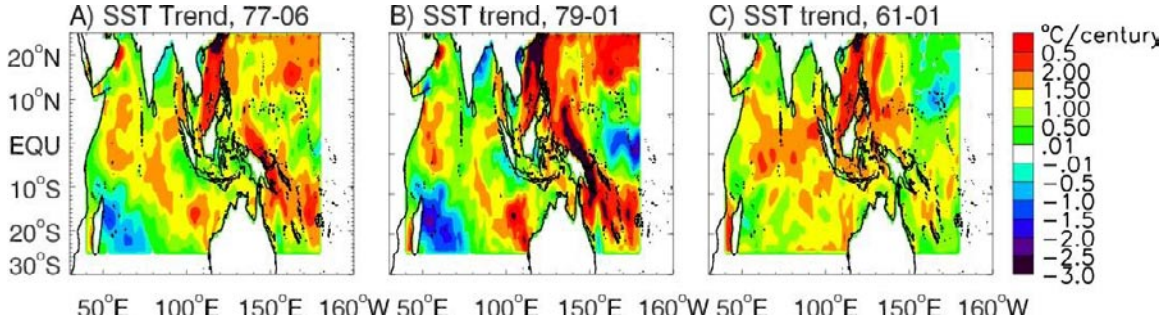
A) SST Trend, 77-06
B) SST trend, 79-01
C) SST trend, 61-01
°C/century
0.5
2.00
1.50
1.00
0.50
.01
-.01
-0.5
-1.0
-1.5
-2.0
-2.5
-3.0
20°N
10°N
EQU
10°S
20°S
30°S
50°E 100°E 150°E 160°W

Fig. S6